

Crystal growth and magnetic behavior of CeCl₃

Nashra Pistawala¹, Suman Karmakar², Rajeev Rawat² and Surjeet Singh*¹

¹Department of Physics, Indian Institute of Science Education and Research, Pune 411008

²UGC-DAE Consortium for Scientific Research, University Campus, Khandwa Road, Indore 452 001

* surjeet.singh@iiserpune.ac.in

Abstract

We have grown high-quality single crystals of CeCl₃ and characterised them using single-crystal x-ray diffraction and Laue diffraction techniques. CeCl₃ crystallizes in a trigonal crystal structure with space group P-3 (No. 147). The magnetic susceptibility shows a broad maximum centred around 50 K. Upon cooling further, the susceptibility rises sharply in a Curie-Weiss manner due to the crystal field split lowest Kramers doublet $|5/2, \pm 5/2\rangle$ with an effective spin 1/2 and a very weak coupling between the Ce moments (Weiss temperature ~ 0.2 K). The magnetic specific heat or C_{4f} shows a Schottky anomaly around 30 K due to the first excited crystal field level located around 58 K. Interestingly, CeCl₃ shows a hint of magnetic field-induced transition in the heat capacity near 2K.

I. Introduction

Quantum antiferromagnets have garnered enormous attention in the past few years. They exhibit exotic phases at low temperatures, including, the much-celebrated Quantum Spin Liquid (QSL) state characterized by fractional excitations and long-range entanglement. The triangular and Kagome lattice antiferromagnets are ideal platforms to realize a QSL phase. In 2009, Kitaev proposed an exactly solvable model for spin 1/2 on a honeycomb lattice, the ground state of which is QSL. Unlike geometric frustration, where the frustration arises due to the geometry of the underlying lattice, in the Kitaev model it is the bond-dependent Ising like interactions that gives rise to a strong frustration. The iridates (e.g., Na₂IrO₃) and the ruthenates (e.g., RuCl₃) have been extensively studied to investigate the interesting physics of the Kitaev model [1,2]. Recently, YbCl₃, a rare-earth trichloride, has

also attracted attention as a quantum antiferromagnet with a honeycomb lattice of the Yb^{3+} ions in a Kramer's doublet ground state ($J_{\text{eff}} = 1/2$) [3]. YbCl_3 belongs to the rare-earth trichloride family with general formula RCl_3 ($\text{R} = \text{Rare earth element}$). While the heavier rare-earth members ($\text{R} = \text{Tb to Lu}$) of this series crystallize with a monoclinic structure with R^{3+} ions forming a honeycomb lattice, the lighter members ($\text{R} = \text{La to Gd}$) crystallize with a hexagonal structure where the R^{3+} ions are arranged on triangular plaquettes that are stacked such that a chain of R^{3+} ions run parallel to the c -axis [4]. Here, we focus on the member CeCl_3 of this series. Both Yb^{3+} and Ce^{3+} are Kramer's ions but while Yb^{3+} is just one short of a completely filled f -shell, Ce^{3+} has only one electron in the f -shell. The previous work on CeCl_3 has concentrated on the low-temperature behaviour of Ce^{3+} moments in the temperature range 0.1 K to 4.2 K, and in magnetic fields up to 14 kOe using the magnetic susceptibility and specific heat probes [5]. The Cl Nuclear Quadrupole Resonance (NQR) on some rare-earth trichlorides and tribromides has also been reported previously [6]. According to these reports, CeCl_3 probably orders antiferromagnetically around 0.11 K, indicating the presence of a very weak exchange between the Ce^{3+} spins. The specific heat at low temperature apparently also shows a strong sample dependence, which has been attributed to the presence of impurities [5]. The magnetic susceptibility or specific heat of CeCl_3 above 4.2 K are unreported to the best of our knowledge.

Here, we report the crystal growth and structural and physical characterizations of CeCl_3 . The mm-size, transparent, high-quality crystals were grown by the modified Bridgman method. These crystals are characterized using powder and single-crystal x-ray diffraction, and Laue diffraction. The magnetic susceptibility and specific heat are measured from liquid Helium temperature to near room temperature. The susceptibility shows a broad peak centred at 50 K. The specific heat shows an upturn upon cooling below 4 K, but no peak could be seen down to a temperature of 2 K. The effect of magnetic field on the low-temperature specific heat has been studied.

II. Experimental Methods

The crystals of rare-earth trichlorides can be grown using the chemical vapour transport method employing AlCl_3 as the transporting agent [7]. In this reaction, the rare-earth oxides are first reacted with AlCl_3 to form corresponding anhydrous rare-earth trichlorides. These are then further reacted with an excess AlCl_3 through a reversible reaction to form gaseous complexes, including $\text{RAl}_3\text{Cl}_{12}$ and $\text{RAl}_4\text{Cl}_{15}$. These gaseous complexes, having a significantly high vapour pressure, are transported to the colder end of the tube, where mm-

sized transparent crystals of RCl_3 can be extracted. Mroczkowski et al. reported the single crystal growth of EuCl_3 using the vertical Bridgman method in the presence of Cl_2 gas under pressure [8]. The anhydrous rare-earth trichlorides RCl_3 in general and CeCl_3 in particular are highly sensitive to moisture and readily form $\text{RCl}_3 \cdot x\text{H}_2\text{O}$ upon coming in contact with the ambient air. It is difficult to grow large, transparent single crystals of rare-earth trichlorides from a melt as the adsorbed moisture, when not carefully removed, reacts with RCl_3 at elevated temperatures leading to a formation of various oxychlorides (e.g., REOCl) which makes the melt hazy. The grown crystal in such cases also has a hazy appearance with multiple cracks. It is, therefore, necessary to remove the adsorbed moisture either by dehydration under a dynamic vacuum at slow rate or by chlorination of the melt using a mixture of ultra-pure argon gas and CCl_4 [9]. A similar method has been described for the crystal growth of CeCl_3 [5].

In this work, high-quality single crystals of anhydrous CeCl_3 are grown from a stoichiometric melt using the static Bridgeman method. The anhydrous CeCl_3 powder (ultra-dry, Purity 99.9%, Alfa Aesar) was stored and handled in an argon filled glove box with O_2 and H_2O level less than 0.1 ppm at all times. The as-purchased powder was further pulverized and filled in a quartz ampoule that was carefully dehydrated by preheating overnight at 1000°C . The loaded ampoule was removed from the glove box and connected to a turbomolecular pump. The other end of the ampoule (where the charge is located) is then introduced in a furnace whose temperature was gradually increased to 230°C . After heating at this temperature for 24 h under dynamic vacuum, the ampoule was allowed to cool down to the room temperature and flame sealed while being evacuated. The sealed ampoule is then placed in a vertical tubular furnace with a temperature gradient. The furnace was heated to 870°C , which is higher than the melting point of anhydrous CeCl_3 (817°C), at a rate of 50°C/h and allowed to dwell at this temperature for 12 h. After this, the furnace was slowly cooled to 750°C at a rate of 0.3°C/h and finally cooled down to room temperature at a rate of 50°C/h . Shiny transparent crystals, few mm in size were carefully extracted from the ampoule.

Single crystal X-ray diffraction was carried out using a Bruker Smart Apex Duo diffractometer at 100 K using $\text{Mo K}\alpha$ radiation ($\lambda = 0.71073 \text{ \AA}$). The total exposure time was 2.01 h. The frames were integrated using the Bruker SAINT software package [13] using a narrow frame algorithm. Data were corrected for absorption effects using the

multiscan method (SADABS) [14]. The structure has been solved and refined using the Bruker SHELXTL software package.

The grown crystals were oriented using a Laue camera (Photonic Science, UK) in backscattering geometry using Tungsten as a source material ($\lambda = 0.35 \text{ \AA} - 2.5 \text{ \AA}$, accelerating voltage 30 kV, Tube current 0.3 mA). The Laue pattern was analysed using Orient Express 3.4 (V 3.3) software package.

The Specific-heat measurements were done using the relaxation method in a Physical Property Measurement System (PPMS), Quantum Design, USA. A small piece of crystal was cut into a 2 mm by 2 mm piece and mounted on the heat capacity sample holder using a low-temperature Apizon N grease. The addenda (heat capacity of sample holder and Apizon N grease) was measured before loading the sample. Sample degradation from moisture effect is minimized by handling, weighing and cutting of CeCl_3 crystal inside the glove box. The magnetic susceptibility was measured at the UGC-DAE centre, Indore, using a VSM probe of a PPMS, Quantum design USA. A single-crystal, approximately 4.1 mg, was mounted on a brass sample holder using the non-magnetic GE Varnish.

III. Results and Discussion

1. Single Crystal growth

A representative image of the crystals grown in our study is shown in Fig. 1 (inset). The crystals are transparent in the form of thin sheets with a typical sheet area of about few mm^2 . The x-ray diffraction in the Bragg Brentano geometry recorded from this surface is shown in Fig.1, the main panel. The only reflections that are seen are those corresponding to the *bc*-plane, suggesting that the specimen being investigated is a single crystal of high quality with *a*-axis along the direction of x-ray beam. This was further confirmed using the x-ray Laue diffraction, where sharp Laue spots were observed, which suggest that the grown crystals are of high quality.

1. Single Crystal X-ray diffraction

A small single crystal specimen was selected for Single Crystal X-ray Diffraction (SCXRD). Table 1 gives the summary of crystallographic parameters. Table 2 summarizes the data collection and structure refinement parameters. Table 3 shows the atomic

coordinates and isotropic atomic displacement parameters. As shown in Table 1, the lower values of R-factors and the goodness of fit is close to 1, which indicates a perfect agreement of the experimental data with the crystallographic model.

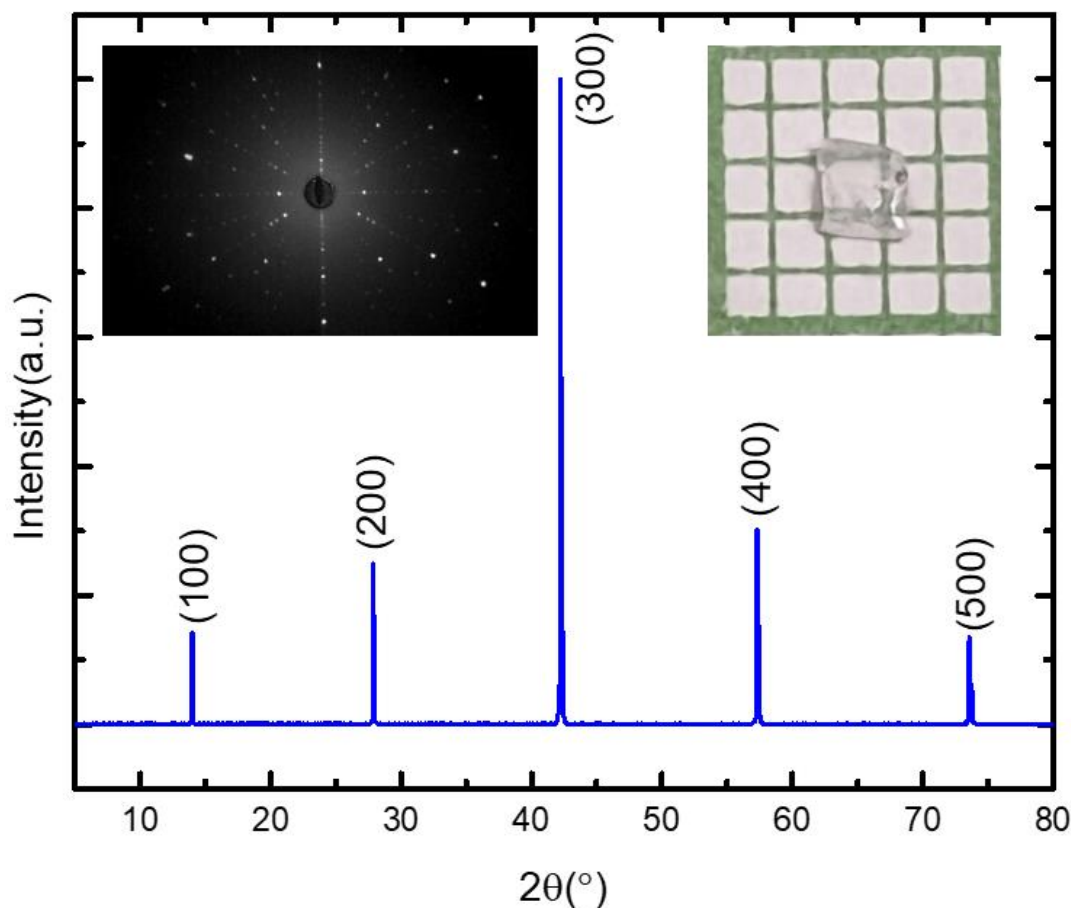


Fig. 1. (a) The x-ray diffraction carried out in the Bragg-Brentano geometry on the specimen shown in the inset. The other inset shows the Laue diffraction pattern from a similar specimen as shown here.

The schematic of the crystal structure of CeCl_3 generated using VESTA [10] is shown in Fig. 2. CeCl_3 crystallizes in a trigonal crystal structure with space group P-3 (No. 147). In this structure, each Ce^{3+} ion is nine-fold coordinated by Cl^- ions, as shown in Fig. 2(a). Of these, three are coplanar with the Ce^{3+} ion. These are labelled 1 to 3. The other six Cl^- ions are located above and below the central Ce^{3+} ion. These are labelled from 4 to 9 in the figure. The polyhedral around the Ce^{3+} are connected via an edge-sharing, forming a ring in the ab -plane. Fig. 2(b) shows the crystal structure as viewed along the b -axis. Each Ce^{3+} ion has two nearest neighbours, each at a distance of 4.326 Å along the c -axis. The exchange paths between any two nearest neighbour is mediated via three $\text{Ce}-\text{Cl}-\text{Ce}$ bridges. The $\text{Ce}-\text{Cl}-\text{Ce}$ bond angle is 95.4° , as shown in Fig. 2(d). The Ce^{3+} ions form a

zig-zag chain along the *c*-axis. Fig. 2(c) shows the crystal structure along the *c*-axis (*ab*-plane), depicting the number of second and third nearest neighbours from the central Ce³⁺ ions. The three next nearest neighbours are shown using magenta circles, each at a distance of 4.7980 Å. The next nearest neighbour interaction is mediated via two Ce–Cl–Cl bridges. The bond angle Ce–Cl–Cl is 110.4°, as shown in Fig. 2(e). In addition, the six third nearest neighbours are shown with red circles drawn around them. Each of these are at a distance of 7.4230 Å from the central Ce ion.

Table 1. Summary of the crystallographic data.

Chemical formula	CeCl ₃
Formula weight	246.47 g/mol
Temperature	273(2) K
Wavelength	0.71073 Å
Crystal system	trigonal
Space group	P -3
Unit cell dimensions	a = 7.4238(11) Å α = 90° b = 7.4238(11) Å β = 90° c = 4.3126(9) Å γ = 120°
Volume	205.84(7) Å ³
Z	2
Density (calculated)	3.977 g/cm ³
Absorption coefficient	12.762 mm ⁻¹
F (000)	218

F (000) is the Structure factor calculated at h = k = l = 0 and indicates the effective number of electrons in the unit cell.

Table 2. Data collection and structure refinement for CeCl₃ single crystals

Theta range for data collection	3.17 to 28.65°
Index ranges	-10 ≤ h ≤ 9, -6 ≤ k ≤ 10, -5 ≤ l ≤ 5

Reflections collected	2703	
Independent reflections	358 [R(int) = 0.0326]	
Coverage of independent reflections	100.0%	
Absorption correction	Multi-Scan	
Structure solution technique	direct methods	
Structure solution program	SHELXT 2014/5 (Sheldrick, 2014)	
Refinement method	Full-matrix least-squares on F ²	
Refinement program	SHELXL-2018/3 (Sheldrick, 2018)	
Function minimized	$\Sigma w(F_{oo}^2 - F_{cc}^2)^2$	
Data / restraints / parameters	358 / 0 / 14	
Goodness-of-fit on F ²	1.189	
Final R indices	358 data; I>2σ(I)	R1 = 0.0151, wR2 = 0.0445
	all data	R1 = 0.0151, wR2 = 0.0445
Weighting scheme	$w = \frac{1}{[\sigma^2(F_o^2) + (0.0107P)^2 + 1.6765P]}$ <p style="text-align: center;">where $P = \frac{F_o^2 + 2F_c^2}{3}$</p>	
Extinction coefficient	0.1180(50)	
Largest diff. peak and hole	1.094 and -1.010 eÅ ⁻³	
R.M.S. deviation from mean	0.169 eÅ ⁻³	

F is the structure factor and is proportional to the square root of the intensity of reflections; F_{oo} and F_{oc} are the observed and calculated structure factors, respectively; R1 refers to the Residual Factor, and wR2 is the weighted Residual factor. R.M.S is the abbreviation for Root Mean Square.

Table 3. Atomic coordinates and equivalent isotropic and anisotropic atomic displacement parameter(Å²).

Label	Wyckoff Positions	x/a	y/b	z/c	U(eq)
Ce01	2d	0.666667	0.333333	0.75001(8)	0.00225(18)
Cl02	6g	0.91360(13)	0.30105(14)	0.2501(2)	0.0033(2)

U(eq) is defined as one-third of the trace of the orthogonalized U_{ij} tensor.

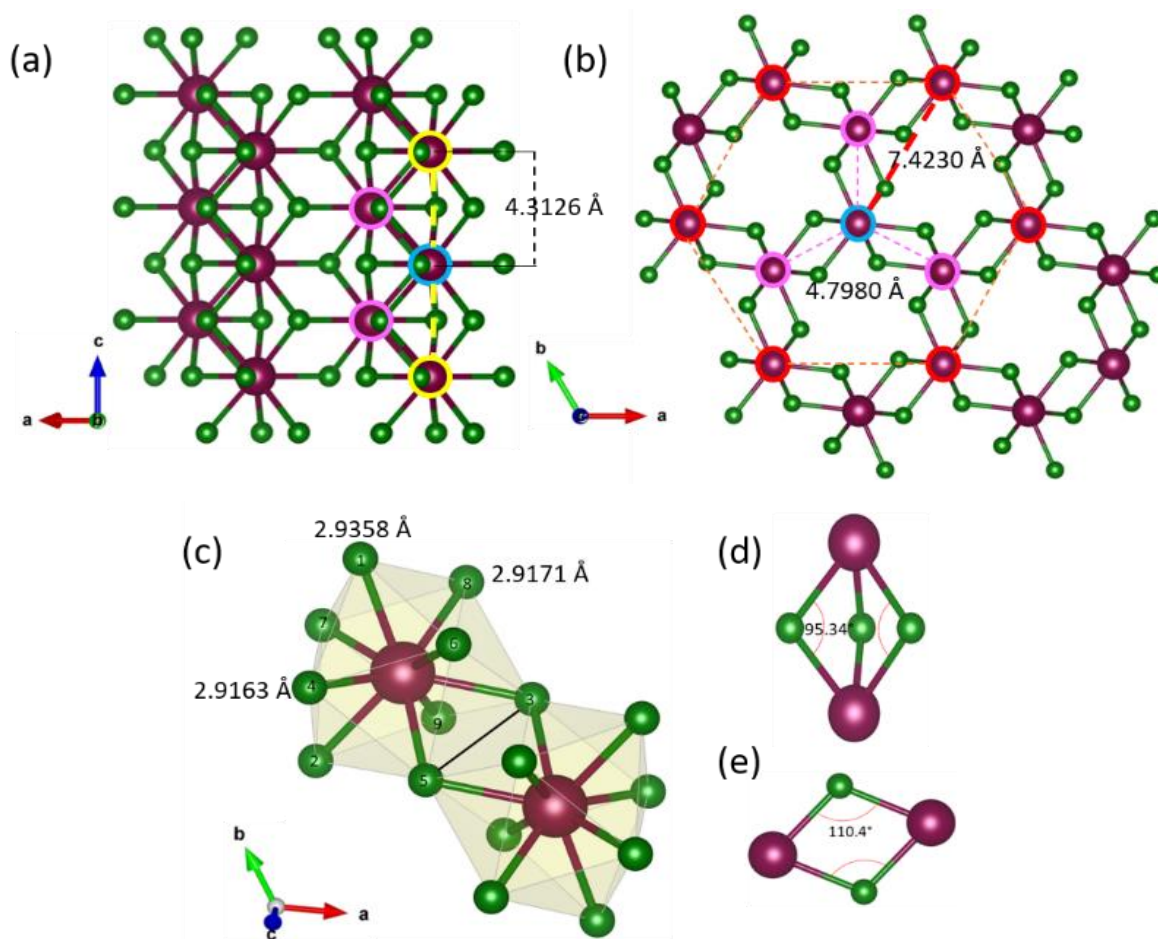


Fig. 2. Schematic representation of crystal structure. The brown balls represent Ce and smaller green balls represent Cl. (a) View along the b -axis (ac -plane) indicating nearest neighbour in yellow circles (b) view along the c -axis (ab -plane) indicating 2nd nearest neighbour in magenta circles and 3rd nearest neighbours in red circles. (c) 9-fold co-ordination of Ce^{3+} ions where Cl⁻ ions numbered 1, 2 and 3 are coplanar and other six Cl⁻ (numbered 4-9) ions are above and below, in the plane perpendicular to a c -axis (d, e) Interaction of Ce^{3+} ions in nearest neighbour and nearest neighbour via 3 Cl⁻ ions (each forming an angle of 95.4°) and 2nd nearest neighbour via 2 Cl⁻ ions (each forming an angle of 110.4°) respectively.

2. Magnetic susceptibility

The magnetic Susceptibility (χ) of a single crystal of CeCl_3 is measured in the temperature range from 4 K to 300 K, as shown in Fig. 3. The magnetic field was applied along the a -axis (i.e., perpendicular to the trigonal c -axis). Since the ordering temperature of CeCl_3 is below 2 K, we expect to see a paramagnetic behaviour over the whole temperature range of our measurement. $\chi(T)$ shows a broad peak around 50 K, and the susceptibility rises sharply again when the sample is cooled further down below 25 K. Generally, a broad peak in the magnetic susceptibility is a characteristic of 1D spin systems, which arises near $k_B T \approx J/2$ where J is the nearest neighbour exchange interaction within the chain. Since J in CeCl_3 is very low, of the order of 0.1 K [6], this scenario can be ruled out. The other possibility is that this peak arises due to the crystal field split Kramers doublets of the lowest $J = 5/2$ manifold of Ce^{3+} . As we shall see shortly, these doublets are located around $\Delta_1 = 58$ K and $\Delta_2 = 167$ K [11], where Δ_1 and Δ_2 are the energy gaps between the ground state and the first and second excited doublet respectively. Below $T < 10$ K, the susceptibility data can be fitted to the modified Curie-Weiss law $\chi = \chi_0 + \frac{C}{(T - \theta_{CW})}$. The fitting is shown in the inset of Fig. 3. The best fit yields $\chi_0 = 5.15 \times 10^{-4}$ emu/mol, $\theta_{CW} = 0.2$ K and $\mu_{eff} = 0.5 \mu_B$. Further, by using $\mu_{eff} = g\sqrt{J(J+1)}$ where g is 0.2 from the previous ESR study ($g_{\parallel} \approx 0.2$ and $g_{\perp} \approx 4.04$ with respect to the c -axis) [12], we obtained $J \approx \frac{5}{2}$. This suggests that the ground state of Ce^{3+} in CeCl_3 is a Kramer's doublet $\pm 5/2$.

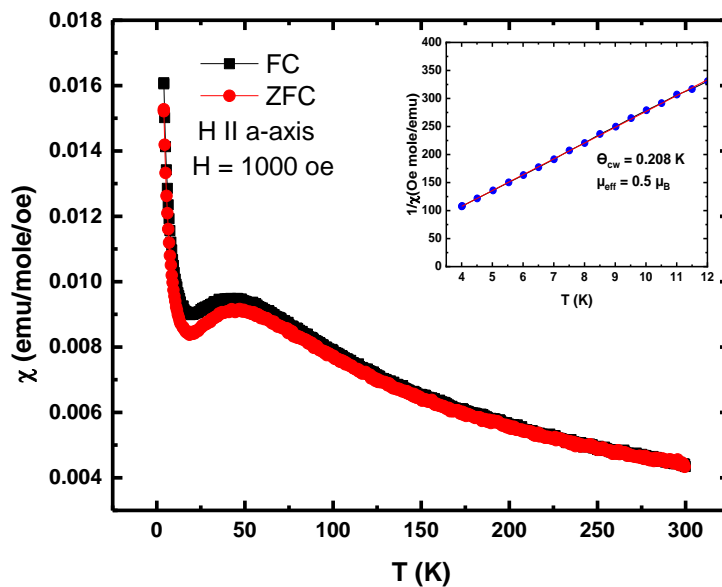


Fig. 3. (a) Susceptibility χ of CeCl_3 for field applied parallel to a-axis. Inset shows the $\chi^{-1}(T)$ fitting to Curie-Weiss law in the low-temperature region.

3. Specific heat

The Specific heat of CeCl_3 is measured from 300K down to 2K in zero field as shown in the inset of Fig. 4. A small but noticeable upturn is seen below 4 K. To further investigate the origin of this upturn, a field of 3 T is applied parallel to the crystallographic a-axis. Interestingly, in the presence of applied field, the upturn becomes more pronounced, and its onset shifted to higher temperatures. Upon further increasing the magnetic field to 8 T, the specific heat started rising upon cooling below 10 K. However, the measurements stopped around 4.5 K as the specimen shattered into small pieces when cooled below this temperature in the presence of 8 T field. This may be an indication of a field induced transition for $H \parallel a$ orientation. The zero-field data of our sample agrees with previous study where the specific heat of CeCl_3 and LaCl_3 was reported below 4.2 K [5]. Upon heating the sample, the specific heat rises attaining the Dulong-Petit value of $3nR$ ($\approx 100 \text{ J mol}^{-1} \text{ K}^{-1}$) where $n = 4$ is number of atoms per formula unit. The reported low-temperature specific heat data of LaCl_3 below 4.2 K is fitted using Debye model T^3 law, from which we obtained $\theta_D \cong 248 \text{ K}$. Assuming the same Debye temperature for its magnetic analogue CeCl_3 , we can estimate C_{4f} above and below 4.2 K by subtracting the measured specific heat of CeCl_3 from that of LaCl_3 , extrapolated up to the higher temperatures using the Debye integral given by equation (1).

$$C_D(T) = 9R \left(\frac{T}{\theta_D} \right)^3 \int_0^{\frac{\theta_D}{T}} \frac{x^4 e^x dx}{(e^x - 1)^2} \quad (1)$$

The extrapolated C_P of LaCl_3 is shown in Fig. 5a using red colour. Interestingly, the extrapolated data overshoots the specific heat of CeCl_3 above 40 K which shows that the extrapolation does not work at high temperatures. There could be various reasons to it, including the role of optical branches in the phonon spectrum. The small mass difference between Ce and La will only have a marginal effect (approximately 0.7%). The other possibility that we looked into was to extrapolate to low temperatures the measured specific heat of CeCl_3 using a Debye-Einstein model. However, since the position of higher lying crystal field levels is not known with certainty, attributing the entire specific heat at high temperatures to phonons is not justifiable. Attempts to fit the specific heat above 4 K using a model consisting of phonons and Schottky contributions also did not converge due to large number of parameters. We therefore decided to stick to this simplest model where the

extrapolated specific heat of LaCl_3 below about 40 K—a temperature not too high to presumably excite the optical modes—would be closest the actual phonon specific heat of CeCl_3 . Hence, we used Debye integral with the estimated θ_D as a rough estimate of the lattice contribution in the low-temperature range to obtain the specific heat associated with the 4f electrons of Ce^{3+} . The Specific heat data of CeCl_3 and extrapolated data for LaCl_3 below 35 K is shown in Fig. 5(a) and $C_{4f} = C_{\text{CeCl}_3}(\text{measured}) - C_{\text{LaCl}_3}(\text{extrpolated})$ is shown in Figure 5(b). The upturn below 2 K is due to the short-range ordering of Ce^{3+} ions and the broad peak centered around 30 K is attributed to the Schottky anomaly due to the splitting of $J = 5/2$ multiplet under the influence of crystal field effects. The broad peak is fitted using a two-level Schottky equation given by:

$$C_{\text{Schottky}} = R \left(\frac{\Delta_1}{T} \right)^2 \frac{e^{-\Delta_1/T}}{(1+e^{-\Delta_1/T})^2}$$

This gives a rough estimate for the energy of the first excited state doublet from the ground state (designated as Δ_1 in the equation) as 58 K. This value is in good agreement with the previous estimate from the variation of C_{4f} between 3.5 and 4.2 K [5].

A more interesting feature emerge in the presence of applied magnetic field. In ref. [5] the low temperature specific heat (below 4.2 K) is measured only up to 1.2 T, the behaviour under high-field was not known from the previous work. In low fields and below 4.2 K [5], the effect of applied field was found to as follows: the sharp peak in the specific heat at 0.11 K, presumably due to the antiferromagnetic ordering of Ce spins, become rounded in the presence of applied magnetic fields and shifts to higher temperatures with increasing field (located around 1.5 K in a field of 1.2 T with the peak C_P/T value of $\approx 1.5 \text{ J mol}^{-1} \text{ K}^{-2}$). This may be attributed to the effect of widening of the energy gap between the exchange split lowest $\pm 5/2$ Kramers doublet under an applied magnetic field as the Zeeman energy is of the same order of magnitude as the exchange energy. However, under a field of 3 T the specific heat starts rising very sharply below 4.2 K attaining a value exceeding $C_P/T = 1.5 \text{ J mol}^{-1} \text{ K}^{-2}$ at the lowest temperature (2 K) without any peak (Fig. 4). Upon increasing the magnetic field further to 8 T, a sharp rise in the C_P/T can be seen below 8 K. However, upon further cooling the measurements stopped around 4.5 K. Upon removing the sample puck, we found that the sample had shattered into numerous small pieces. Since the specific heat measurements are done under high vacuum, we cannot attribute this to sample decomposition. It is possible that CeCl_3 exhibits a field induce magnetic transition and further studies should be done to understand this better.

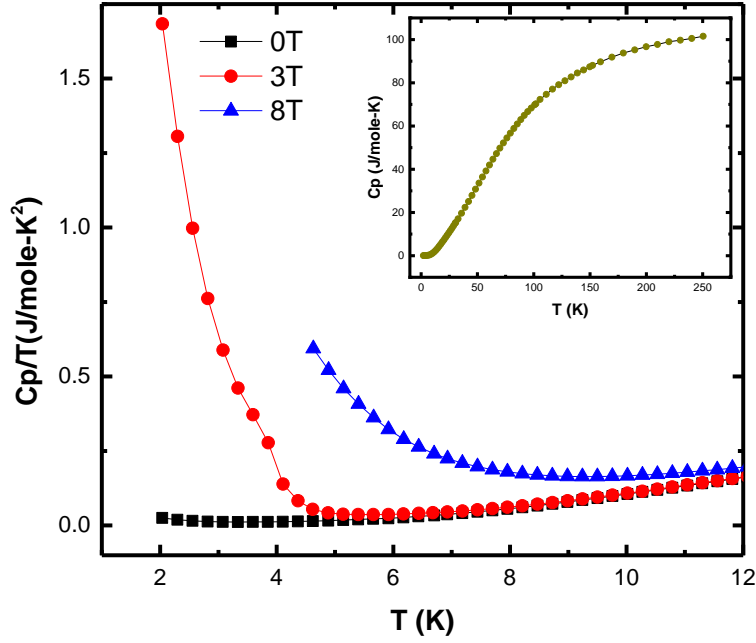


Fig. 4. Temperature variation of low-temperature specific heat measured under different applied magnetic fields. The inset shows the specific heat of CeCl_3 in the temperature range of 2 K – 250 K. The measurements under 8 T field could not be completed as the sample shattered into small pieces upon cooling below 4.5 K in the presence of 8 T field.

Ff

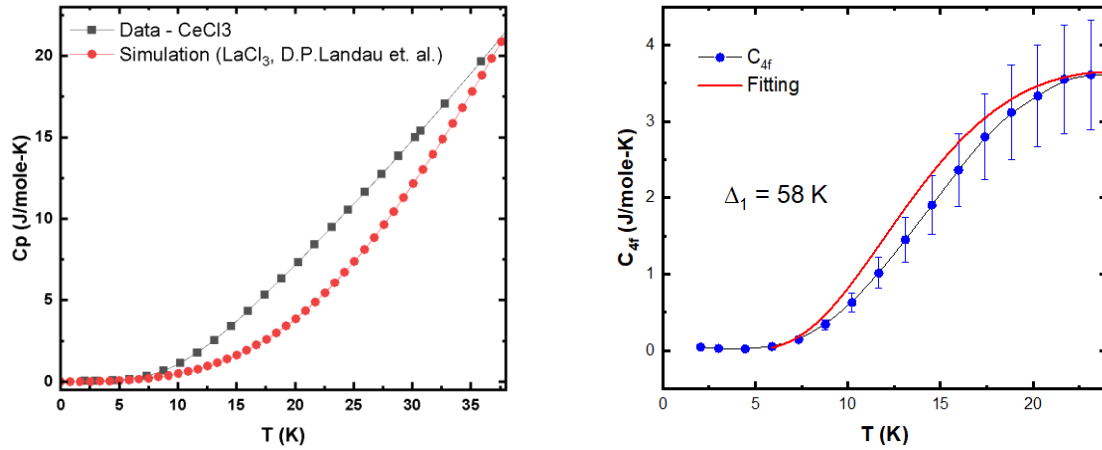


Fig. 5. (a) Variation of Zero field Specific heat data of CeCl_3 single crystals (filled black squares) and LaCl_3 data (filled red circles) [5] (b) Contribution to the Specific heat from 4f electrons obtained from subtracting the specific heat of LaCl_3 from CeCl_3 and fit using the two-level Schottky model (see text for details).

4. Summary and conclusions

High-quality single crystals of CeCl_3 were grown using the static Bridgman method. The grown crystals were characterized using single-crystal x-ray diffraction, x-ray diffraction from a single crystal in the Bragg Brentano geometry, and Laue diffraction. We found that CeCl_3 crystallizes in a trigonal crystal structure with space group P-3 (No. 147). The thermal and magnetic properties are studied using heat capacity and magnetic susceptibility probes. The magnetic susceptibility measured along the a -axis shows a broad susceptibility peak centered around 50 K. The low temperature ($T < 10$ K) susceptibility is fitted using the modified Curie-Weiss law. The Weiss temperature is found to be 0.2 K suggesting that the Ce spins are very weakly coupled. The effective magnetic moment obtained from the Curie-Weiss fit confirms that the crystal field split ground state of Ce^{3+} is $|\frac{5}{2}, \frac{\pm 5}{2}\rangle$. The specific heat measured in the temperature range of 2 K to 300 K is devoid of any sharp anomalies. The analysis of the specific heat suggests that the first excited Kramers doublet is situated around 58 K. Further investigations using neutron diffraction, inelastic neutron scattering, and Muon spin relaxation technique are needed to fully understand the intriguing magnetic and thermal behaviour of CeCl_3 .

References

- [1] S. Widmann, V. Tsurkan, D.A. Prishchenko, V.G. Mazurenko, A.A. Tsirlin, A. Loidl, Thermodynamic evidence of fractionalized excitations in α - RuCl_3 , *Phys. Rev. B.* 99 (2019) 094415. <https://doi.org/10.1103/PhysRevB.99.094415>.
- [2] J. Chaloupka, G. Khaliullin, Magnetic anisotropy in the Kitaev model systems Na_2IrO_3 and RuCl_3 , *Phys. Rev. B.* 94 (2016) 064435. <https://doi.org/10.1103/PhysRevB.94.064435>.
- [3] J. Xing, E. Feng, Y. Liu, E. Emmanouilidou, C. Hu, J. Liu, D. Graf, A.P. Ramirez, G. Chen, H. Cao, N. Ni, Néel-type antiferromagnetic order and magnetic field–temperature phase diagram in the spin-1/2 rare-earth honeycomb compound YbCl_3 , *Phys. Rev. B.* 102 (2020) 014427. <https://doi.org/10.1103/PhysRevB.102.014427>.
- [4] W.H. Zachariasen, Crystal chemical studies of the 5f-series of elements. I. New structure types, *Acta Crystallogr.* 1 (1948) 265–268. <https://doi.org/10.1107/s0365110x48000703>.
- [5] D.P. Landau, J.C. Doran, B.E. Keen, Thermal and Magnetic Properties of CeCl_3 , *Phys. Rev. B.* 7 (1973) 4961–4979. <https://doi.org/10.1103/PhysRevB.7.4961>.
- [6] J.H. Colwell, B.W. Mangum, D.B. Utton, Low-temperature magnetic properties of some hexagonal rare-earth trihalides, *Phys. Rev.* 181 (1969) 842–854.

<https://doi.org/10.1103/PhysRev.181.842>.

- [7] H. Gunsilius, Darstellung von Selten- Erd-Trichloriden über chemischen Transport mit Aluminiumtrichlorid H. GUNSILIUS~, W., 650 (1987) 35–40.
- [8] S. Mroczkowski, Preparation of single crystals of EuCl_3 and related polyvalent halides, *J. Cryst. Growth.* 6 (1970) 147–150. [https://doi.org/https://doi.org/10.1016/0022-0248\(70\)90033-3](https://doi.org/https://doi.org/10.1016/0022-0248(70)90033-3).
- [9] M. Voda, M. Al-Saleh, G. Lobera, R. Balda, J. Fernández, Crystal growth of rare-earth-doped ternary potassium lead chloride single crystals by the Bridgman method, *Opt. Mater. (Amst).* 26 (2004) 359–363. <https://doi.org/https://doi.org/10.1016/j.optmat.2003.12.019>.
- [10] K. Momma, F. Izumi, VESTA 3 for three-dimensional visualization of crystal, volumetric and morphology data, *J. Appl. Crystallogr.* 44 (2011) 1272–1276. <https://doi.org/10.1107/S0021889811038970>.
- [11] D.M. Juraschek, T. Neuman, P. Narang, Giant effective magnetic fields from optically driven chiral phonons in $4f$ paramagnets, *Phys. Rev. Res.* 4 (2022) 013129. <https://doi.org/10.1103/PhysRevResearch.4.013129>.
- [12] C.A. Hutchison, E. Wong, Paramagnetic resonance in rare earth trichlorides, *J. Chem. Phys.* 29 (1958) 754–760. <https://doi.org/10.1063/1.1744587>.
- [13] Bruker APEX3, Analytical X-ray Instruments Inc., Madison, Wisconsin, USA, 2016.
- [14] Bruker SAINT, Analytical X-ray Instruments Inc., Madison, Wisconsin, USA, 2016.